

PriorMotion: Generative Class-Agnostic Motion Prediction with Raster-Vector Motion Field Priors

Kangan Qian¹, Xinyu Jiao¹, Yining Shi¹, Yunlong Wang¹, Ziang Luo¹, Zheng Fu¹, Kun Jiang¹, Diange Yang¹

¹Tsinghua University, China

{qka23, jiaoxinyu, syn21, luoza24, fu-z20, jiangkun, ydg}@mails.tsinghua.edu.cn

Abstract

*Reliable perception of spatial and motion information is crucial for safe autonomous navigation. Traditional approaches typically fall into two categories: object-centric and class-agnostic methods. While object-centric methods often struggle with missed detections, leading to inaccuracies in motion prediction, many class-agnostic methods focus heavily on encoder design, often overlooking important priors like rigidity and temporal consistency, leading to suboptimal performance, particularly with sparse LiDAR data at distant region. To address these issues, we propose **PriorMotion**, a generative framework that extracts rasterized and vectorized scene representations to model spatio-temporal priors. Our model comprises a BEV encoder, an Raster-Vector prior Encoder, and a Spatio-Temporal prior Generator, improving both spatial and temporal consistency in motion prediction. Additionally, we introduce a standardized evaluation protocol for class-agnostic motion prediction. Experiments on the nuScenes dataset show that PriorMotion achieves state-of-the-art performance, with further validation on advanced FMCW LiDAR confirming its robustness.*

1. Introduction

Autonomous driving systems[1, 20] demand highly precise spatial perception, including position information [10], semantic classification [31], and motion behavior [22], which are crucial for ensuring safety and comfort in open-world scenarios [1, 26, 41]. The traditional paradigm of object-centric methods models motion behavior estimation as a trajectory prediction task[5, 6, 8, 23, 54], which, despite its maturity, falters in open environments due to its reliance on detection-tracking-prediction pipelines that are ill-equipped to handle inexhaustible categories of traffic participants critical for system safety[49].

Recently, class-agnostic methods have emerged as a promising alternative by jointly performing semantic clas-

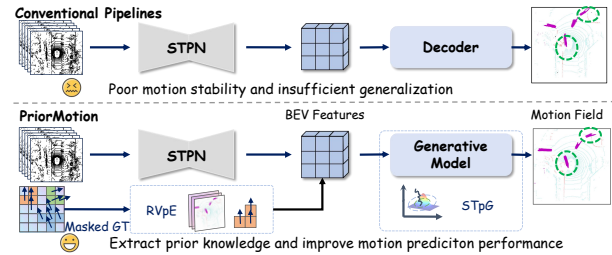


Figure 1. Comparison of PriorMotion with conventional pipelines. **Top row:** Previous framework, which adopts a serial design of encoder-decoder pipeline. **Bottom:** Our approach leverages prior knowledge from the motion field ground truth, modeling motion prediction as a future generation task in a structured latent space.

sification and motion prediction through a Bird’s Eye View (BEV) occupancy grid approach[29, 37, 49]. BE-STI[44], ST-Transformer[46] have shown significant performance improvements with the enhanced backbone. On the other hand, while showing promise, these methods have demonstrated suboptimal performance from a visualization standpoint. The predicted motion field suffers from poor spatial stability (e.g., grids belonging to the same instance should exhibit consistent displacement[9]) and weak temporal consistency. Additionally, for distant regions, the inherent sparsity of point cloud inputs lead to inaccurate predictions. Exploring methods to mitigate these drawbacks could lead to a deeper understanding of driving scenarios and potentially enhancing the performance of motion planning and further providing smooth user experience.

Drawing inspiration from the thought-provoking question posed by LeCun [18]: “*Why can an adolescent learn to drive a car in about 20 hours of practice and know how to act in many situations he/she has never encountered before?*”, we delve into the core principles of human perception and cognitive skills [52]. Human learning demonstrates that leveraging prior knowledge enables better generalization to new and unseen scenarios.

While current methods have primarily focused on encoder architectures, they have largely overlooked the role of the incorporation of prior knowledge about the motion field. For instance, the braking action of a leading vehicle can trigger a similar response in a following vehicle. Ad-

ditionally, future motion displacements in such scenarios are often highly structured and continuous, such as linear and sequential movements. These patterns are challenging to capture with current methods, leading to poor prediction performance. Our goal in this paper is to explore a better way to integrate prior information into existing pipelines, utilizing a generative framework to enhance class-agnostic perception and motion prediction performance.

Our proposed framework, **PriorMotion**, leverages structured priors inherent in motion fields, which are often underutilized in existing methods. As illustrated in Fig. 1, the previous framework follows a conventional pipeline consisting of a backbone encoder and a motion decoder, which struggles with motion stability and generalization. In contrast, PriorMotion introduces two key modules: the **Raster-Vector prior Encoder (RVpE)** and the **Spatial-Temporal Gaussian prior Generator (STpG)**. The **RVpE** module combines a Raster prior Encoder (**RpE**), which extracts dense spatio-temporal information, with a Vector prior Encoder (**VpE**), which captures instance-level interaction cues for future motion. To model these priors, a Variational Autoencoder is employed, which maps motion field ground truth onto spatio-temporal Gaussian distributions. This generative framework allows us to model future motion as a task in a structured latent space. Additionally, to handle the heterogeneity of tasks, we use a spatial GRU[38] for autoregressive modeling of motion in the latent space, while semantic classification tasks are directly modeled through single spatial Gaussian features. Our contributions are summarized as follows:

- We propose **PriorMotion**, a pioneering generative framework for class-agnostic motion prediction that fully leverages structured priors from motion fields, significantly enhancing traditional pipelines.
- We introduce the RVpE and STpG to efficiently extract prior knowledge. RVpE fuses dense grid-level and sparse instance-level interaction information, while STpG captures spatial-temporal priors through Gaussian distributions, resulting in improved spatial and temporal consistency in motion prediction.
- Extensive experiments on the nuScenes and our private FMCW LiDAR benchmark demonstrate that **PriorMotion** surpasses previous SOTA methods. Additionally, we introduce new metrics for a more comprehensive evaluation of class-agnostic motion prediction.

2. Related Work

2.1. Motion Prediction

Motion prediction methods focus on extracting spatial and semantic information to predict agents' future trajectories from past observations[19]. These approaches are broadly categorized into object-centric and class-agnostic types.

Object-centric methods typically involve detection[17, 27, 28, 36, 51], tracking[15, 33, 39], and prediction[7, 48, 50], arranged in a cascaded pipeline where each module sequentially feeds into the next. However, these methods rely heavily on object detectors, which may struggle in open-set scenarios with unknown objects. End-to-end multitask frameworks[34, 45] attempt to mitigate this by jointly predicting motion and perception, though they often encounter training and optimization challenges. **Class-agnostic** methods, on the other hand, directly predict cell classification and motion fields in Bird's Eye View (BEV) without relying on upstream detection[21, 29, 42, 43]. These approaches are more robust in open-world scenarios, effectively perceiving objects unseen during training. MotionNet[49] laid the foundation for grid-based spatial perception, followed by PillarMotion[25], which used cross-sensor self-supervision with RGB optical flow, achieving significant improvements in motion prediction accuracy. BE-STI[44] introduced a spatio-temporal bidirectional enhancement encoder for separate decoding of grid semantics and motion, while ST-Transformer[47] applied spatio-temporal attention to enhance feature extraction. However, most existing methods focus on encoder design, with limited attention to utilizing prior knowledge from motion fields.

In contrast, our generative framework integrates prior knowledge from motion field data using spatio-temporal Gaussian distributions, enhancing the decoder's ability to produce more accurate and adaptable predictions across diverse motion patterns. To further advance the evaluation of class-agnostic methods, a comprehensive evaluation protocol is proposed. This includes novel metrics that assess not only traditional metrics[44, 47, 49], but also spatial stability and long-range prediction accuracy, providing a more comprehensive assessment of class-agnostic motion prediction.

2.2. Generative Framework

Generative methods have been widely applied in various fields, including image processing[32], text generation[2], and malware classification[3]. In autonomous driving, their utility in trajectory prediction is particularly noteworthy[12, 40, 53, 55]. For example, Social GAN[12] integrates adversarial training for pedestrian motion forecasting, while TrajGen[53] generates diverse and realistic trajectories to enhance system adaptability in complex scenarios. DiffMap[14] is the prior work to use the generative framework with diffusion models to improve map segmentation.

Our work presents a pioneering generative framework tailored for motion prediction, addressing a significant void in the utilization of generative models for class-agnostic motion prediction tasks.

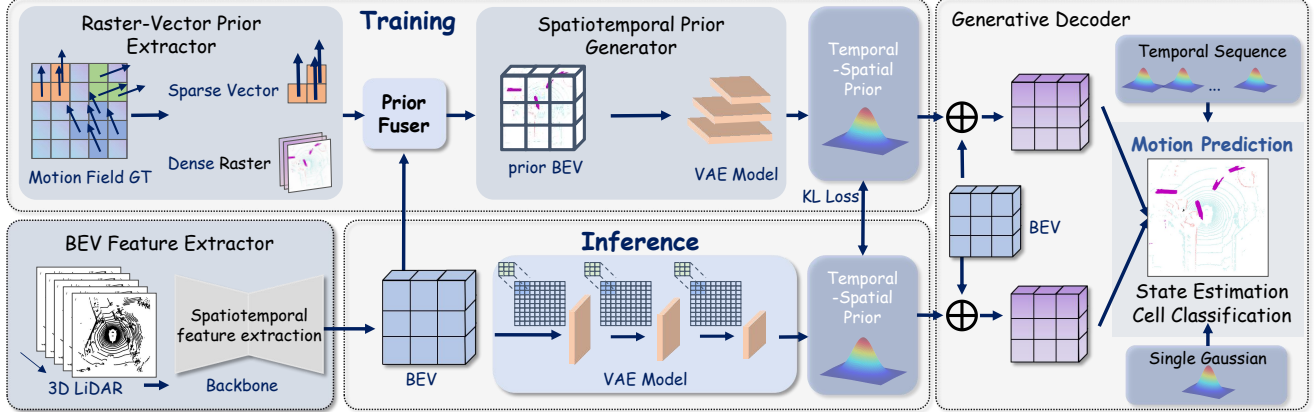


Figure 2. Architecture of **PriorMotion**. The architecture comprises several key components: a BEV Feature Encoder, a Raster-Vector prior knowledge Encoder(RVpE) and a Spatio-Temporal prior Generator(STpG).

3. The proposed Approach

3.1. Problem Formulation

In autonomous driving systems, accurate motion and semantic prediction from LiDAR point clouds is essential. This task involves processing raw, sparse, and nonuniform 3D data to infer spatiotemporal features for both cell classification and motion prediction.

Input data representation. The input to our model is a sequence of LiDAR point clouds, denoted as $P_t = \{\mathcal{P}_t^i\}_{i=1}^{N_t}$, where $\mathcal{P}_t^i \in \mathbb{R}^3$ represents the coordinates of a point at time t , and N_t is the number of points in the cloud. These point clouds are synchronized to the ego vehicle’s coordinate system, following the approach in MotionNet [49].

The point clouds are transformed into a voxelized representation $\mathcal{V}_t \in \{0, 1\}^{H \times W \times C}$, where H , W , and C are the voxel grid dimensions along the X, Y, and Z axes. Non-empty voxels are set to 1, and empty ones to 0.

Output data representation. The model outputs cater to three tasks: motion prediction, cell classification, and state estimation. For motion prediction, we predict the future trajectory of each cell in the BEV pseudo-image as: $\{\mathcal{M}_t = (x_t, y_t) \mid \mathcal{M}_t \in \mathbb{R}^{H \times W \times 2}\}_{t=1}^T$ where \mathcal{M}_t denotes the BEV motion field, and T is the number of predicted frames. For cell classification, we predict the class of each cell at the current time step, represented as $\mathcal{C}_t \in \mathbb{R}^{H \times W \times N_c}$, where \mathcal{C}_t contains the class labels of each cell, and N_c denotes the number of detectable cell categories. For state estimation, we predict the probability of each cell being static, represented as $\mathcal{S}_t \in \mathbb{R}^{H \times W}$, which denotes the static probability for each cell.

Problem formulation. Given a sequence of LiDAR point clouds $\{\mathcal{P}_t\}_{t=1}^T$, our goal is to predict future object positions, classify each cell, and estimate its state in the BEV map. We aim to learn a function f such that:

$$f(\{\mathcal{P}_t\}_{t=1}^T) \rightarrow (\mathcal{M}_t, \mathcal{C}_t, \mathcal{S}_t) \quad (1)$$

where \mathcal{M}_t , \mathcal{C}_t , and \mathcal{S}_t are the predicted motion field, class

labels, and static probabilities, respectively.

3.2. PriorMotion Network

We introduce a novel generative architecture, PriorMotion, designed to enhance motion prediction in autonomous driving. As shown in Fig.2, the architecture comprises three key components: a BEV Feature Encoder(3.2.1), a Raster-Vector prior knowledge Encoder(RVpE)(3.2.2) and a Spatio-Temporal prior Generator(STpG)(3.2.3).

3.2.1 BEV Feature Encoder

The BEV feature Encoder processes multiple frames of voxelized point clouds \mathcal{V}_t . The BEV feature encoder in our framework can be flexibly chosen from various state-of-the-art architectures, including the Spatio-Temporal Pyramid Network (STPN)[49], the Transformer-based Spatio-Temporal Transformer (STT)[47], or the temporally and spatially bidirectional enhanced encoder (TeSE and SeTE) from BE-STI[44]. Using the backbone network, it outputs a BEV feature map $\mathcal{B} \in \mathbb{R}^{H \times W \times C'}$. This encoder is critical for capturing dynamic spatial information across frames, forming the foundation for subsequent modules

3.2.2 Raster-Vector prior Encoder

The prior knowledge extractor in PriorMotion is designed to distill valuable prior knowledge from the motion field, which is crucial for enhancing the network’s performance. Given that class-agnostic methods operate on grid data in the Bird’s Eye View (BEV) pseudo-image, we naturally leverage dense rasterized representations to encode prior knowledge. Additionally, to account for the instance characteristics of objects, we also extract sparse vectorized representations to capture the spatiotemporal interactions between instances. This dual approach ensures a comprehensive integration of prior knowledge. The process consists of two main parts: Raster Prior Encoder and Vector Prior Encoder as illustrated in Fig.3.

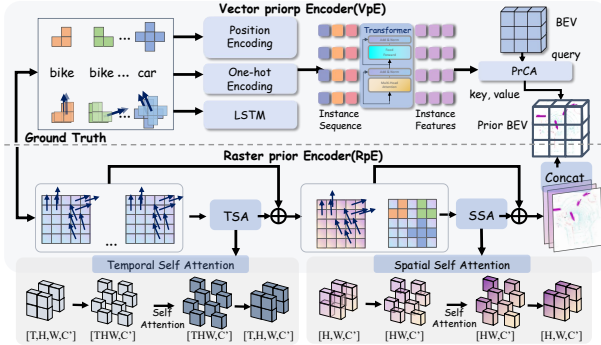


Figure 3. **RVpE** Module. The top row illustrates the Vector Prior Encoder (VpE), which captures sparse spatiotemporal interactions between instances. The bottom row shows the Raster Prior Encoder (RpE), which encodes dense rasterized representations of the motion field to enhance class-agnostic grid predictions.

Raster prior Encoder. For motion information extraction, especially given the temporal nature of the rasterized data, we first apply a Temporal Self-Attention(TSA) module to extract temporal features from the motion field. This operation results in a new feature map $\mathcal{F}(\mathcal{T}_M)$ that captures the temporal dependencies across sequences. After obtaining the temporally enriched feature map, we concatenate it with the category map \mathcal{C} and motion state map \mathcal{S} to form a new feature map.

The newly formed feature map is then passed through a Spatial Self-Attention(SSA) module, which extracts spatial features by modeling the relationships between different locations in the scene. The proposed TSA and SSA with the raster prior knowledge \mathcal{P}_R can be represented as follows:

$$\mathcal{T}_M = \text{TSA}(q = k = v = \mathcal{T}(\mathcal{M})) \quad (2)$$

$$\mathcal{P}_R = \text{SSA}(q = k = v = \mathcal{T}([\mathcal{F}(\mathcal{T}_M), \mathcal{C}, \mathcal{S}])) \quad (3)$$

where $\mathcal{T}(\cdot)$ denotes the projection of query(q),key(k) and value(v), $[\cdot]$ denotes the concatenate operation.

Vector prior Encoder. For extracting the instance-level prior knowledge, we employ an instance sequence representation. Given the motion field with semantic and motion information, we sample a fixed number of grids N along each instance, analogous to polyline sampling on SD maps. Each grid is represented by its coordinates (x_i, y_i) and is associated with a specific grid cell's displacement vector v . We employ sinusoidal embeddings to encode the positional information of these grids, which is crucial for capturing the nuances of the motion field's structure. We leave the details of the sinusoidal embeddings in the appendix.

Each instance is also encoded with a one-hot vector representation for its category, providing semantic context to the instance. Additionally, the displacement is encoded using LSTM which processes the displacement field sequence of dimension $(T, 2)$ and outputs a displacement feature vector of dimension (T, d_M) . The instance sequence

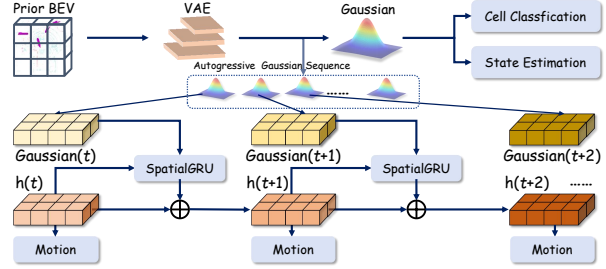


Figure 4. **STpG** Module. The top part illustrates the VAE-based latent prior modeling, where prior BEV are projected into a Gaussian latent space. The bottom part shows the decoding process with spatialGRU, ensuring temporal consistency in the generated motion fields for motion field generation.

$\mathcal{I} \in \mathbb{R}^{bs \times nins \times d_x}$ is then formed by concatenating the positional embeddings, displacement embeddings, category labels for each grid point, resulting in a representation of shape $M \times (N \cdot d + K + T \cdot d_M)$, where M is the total number of grid, K is the number of categories, d is the embedding dimension, and d_M is the dimension of the displacement embeddings.

Transformer encoder for vector priors. Given the instance sequence representation of motion field, we wish to use a Transformer encoder to learn a feature representation for the interactive feature learning. We embed the instance sequence with a MLP-layer, typical of Transformer encoder architectures. This ensures that the discrete, one-hot representation of the cell class can be meaningfully transformed into continuous space. The Transformer Encoder consists of L layers of self-attention, allowing the network to model global relationships between instances with their corresponding motion across the entire scene. The output \mathcal{P}_V is a vector prior knowledge representation of shape $M \times H$, where H is the feature dimension produced by the instance-level self-attention(ISA) mechanism, which can be formulated as follows:

$$\mathcal{P}_V = \text{ISA}(q = k = v = \mathcal{I}) \quad (4)$$

Prior fusion. The fusion of prior knowledge from RVpE is formulated as 5.

$$\mathcal{B}' = [\mathcal{B}, \mathcal{P}_R, \text{PrCA}(q = \mathcal{B}, k = v = \mathcal{P}_V)] \quad (5)$$

After extracting raster and vector prior knowledge, we apply prior cross-attention (PrCA) between the BEV features and vector priors. We then concatenate the enriched BEV features with raster priors, resulting in vector prior-enhanced BEV features. The final fused features $\mathcal{B}' \in \mathbb{R}^{H \times W \times C'}$ combine BEV features from voxelized point clouds and prior knowledge, offering a comprehensive representation for downstream tasks.

3.2.3 Spatio-Temporal prior Generator

The primary objective of motion field prediction is to generate a realistic and high-quality displacement map in the

BEV space. The task can be framed as predicting the future motion field \mathcal{M} based on BEV features \mathcal{B} . Unlike traditional approaches that directly decode the motion field through a simple convolutional decoder, we reformulate this task as a generative problem, $\mathcal{M} \sim p(\mathcal{M} | \mathcal{B})$, to account for the inherent uncertainty in motion prediction. Motion fields exhibit structured patterns (e.g., instance consistency and rigid dynamics). For example, most motion vectors follow steady motion behaviors when vehicles move at constant speeds. Zig-zagging patterns are extremely rare.

To better capture these structured dynamics and make full use of the prior knowledge, we employ a Variational Autoencoder (VAE)-based architecture. This model encodes the BEV features into a probabilistic latent space, resulting in a Gaussian distribution \mathcal{K} with a reduced spatial scale of $(H/4 \times W/4 \times C_{\mathcal{K}})$ to reduce computation costs, where $C_{\mathcal{K}}$ represents the dimensionality of the Gaussian distribution, effectively encapsulating the complex spatio-temporal dynamics.

Motion field prior modeling. We utilize a VAE to project prior BEV into a latent space that captures the structural prior of the scene. This latent space is modeled as a Gaussian distribution, where the VAE encoder outputs the mean μ_f and variance σ_f^2 of the distribution, encapsulating prior knowledge about realistic motion field:

$$p(\mathcal{Z} | \mathcal{M}(\mathcal{B}')) \sim \mathcal{N}(\mu_f, \sigma_f^2) \quad (6)$$

Here, $\mathcal{N}(\mu, \sigma^2)$ represents a Gaussian distribution parameterized by mean μ and variance σ^2 . This learned distribution, $p(\mathcal{Z} | \mathcal{M}(\mathcal{B}'))$, captures the prior knowledge of ground-truth motion field, which is instrumental in enhancing the authenticity of motion prediction.

Spatial-Temporal Gaussian priors. Once the latent prior distribution of the future motion field is obtained, we decode the latent representations into explicit motion fields in the BEV space. A direct approach would involve feeding the latent features into a decoder to generate the motion field, along with cell classification and state estimation. However, such an approach neglects the temporal evolution and interaction dynamics of grids.

To address this, we introduce a spatial gated recurrent unit (SGRU) to incorporate temporal dynamics into the decoding process. This ensures that the generated motion fields are not only spatially coherent but also temporally consistent. The SGGRU models the temporal evolution of rasterized representations in the latent space \mathcal{Z}_s . Specifically, the SGGRU takes the current latent representation z_t and transforms it into the next state, $\text{SGGRU}(z_t) = z_{t+1}$. Subsequently, we decode the motion field for the next time step, \mathcal{M}_{t+1} , using a Feature Selection Decoder with SE layer[13] (explained in appendix), i.e., $\mathcal{M}_{t+1} = d_{SE}(z_{t+1})$. This process models the conditional probability:

$$p(\mathcal{M}_{T+1} | \mathcal{M}_T, \dots, \mathcal{M}_{T+f-1}, \mathcal{Z}_s) \quad (7)$$

For classification tasks, the model decodes the motion field using a single spatial Gaussian distributions with original BEV features. This process models the conditional probability $p(\mathcal{C}, \mathcal{S} | \mathcal{Z}_s)$, the distribution of the classification and state estimation can be formulated as follows:

$$p(\mathcal{C}(\mathcal{M}(\mathcal{B}')), \mathcal{S}(\mathcal{B}') | \mathcal{Z}_s) = \mathcal{B}' \oplus \mathcal{Z}_s \quad (8)$$

where \oplus denotes element-wise addition. We illustrate the proposed STpG in Fig.4.

3.2.4 Loss Function

The PriorMotion model is trained using a composite loss function that optimizes motion prediction, cell classification, state estimation, and motion field priors. For motion prediction, classification, and state estimation, we follow standard practices from [49], with details in the supplementary materials.

Prior loss. We introduce a Kullback-Leibler (KL) divergence loss to model motion field priors. This loss ensures the predicted BEV distribution $p(\mathcal{Z}_s | \mathcal{B})$ matches the ground truth $p(\mathcal{Z}_s | \mathcal{B}')$, enforcing consistency with learned motion priors:

$$L_{\text{prior}} = \text{KL}(p(\mathcal{Z}_s | \mathcal{B}) \| p(\mathcal{Z}_s | \mathcal{B}')) \quad (9)$$

This term improves generalization to unseen motion patterns. The total loss is a weighted sum of individual terms, balancing their contributions during training:

$$L = \lambda_{\text{mot}} \cdot L_{\text{mot}} + \lambda_{\text{state}} \cdot L_{\text{state}} + \lambda_{\text{cls}} \cdot L_{\text{cls}} + \lambda_{\text{prior}} \cdot L_{\text{prior}} \quad (10)$$

where λ_{mot} , λ_{state} , λ_{cls} , and λ_{prior} are hyperparameters controlling the importance of each loss term.

4. Experiment

4.1. Experimental Setup

Dataset. We conduct our experiments on the **nuScenes** dataset[4], a large-scale autonomous driving benchmark that provides comprehensive sensor data, including a 360-degree LiDAR, cameras, and radars. The dataset consists of 1000 scenes, with 850 scenes for training and validation, and 150 scenes for testing. Following the standard split, we use 500 scenes for training, 100 scenes for validation, and 250 scenes for testing. Each scene lasts approximately 20 seconds, with annotations provided at 2Hz and LiDAR point clouds captured at 20Hz. Ground truth bounding box annotations are available for motion prediction.

Implementation details. For fair comparison, the same data preprocessing pipeline is adopted as in [49]. Input point clouds are cropped to the range of $[-32m, 32m] \times [-32m, 32m] \times [-3m, 2m]$ and voxelized with a resolution of $0.25m \times 0.25m \times 0.4m$. Each sequence consists

Method	Backbone	Static		Speed $\leq 5\text{m/s}$		Speed $> 5\text{m/s}$		Motion.S
		Mean \downarrow	Median \downarrow	Mean \downarrow	Median \downarrow	Mean \downarrow	Median \downarrow	Variance \downarrow
StaticModel	Rules	0	0	0.6111	0.0971	8.6517	8.1412	0
FlowNet3D[24]	PointNet	0.0410	0	0.8183	0.1782	8.5261	8.0230	0
HPLFlowNet[11]	BCL	0.0041	0.0002	0.4458	0.0960	4.3206	2.4881	0
PointRCNN[56]	PointNet	0.0204	0	0.5514	0.1627	3.9888	1.6252	0
LSTM-EM[29]	LSTM	0.0358	0	0.3551	0.1044	1.5885	1.0003	0
Pillar.M(L&I)[25]	Pillar.E	0.0245	0	0.2286	0.0930	0.7784	0.4685	-
MotionNet[49]	STPN	0.0262	0	0.2467	0.0961	0.9878	0.6994	0.0267
MotionNet[49] \dagger	STPN	0.0201	0	0.2292	0.0952	0.9454	0.6180	0.0251
MotionNet[43] \ddagger	STPN	0.0271	0	0.2267	0.0945	0.8427	0.5173	-
PriorMotion(Ours)	STPN	0.0285	0	0.2364(↓4.18%)	0.0893	0.8064(↓18.36%)	0.5869	0.0074
ST-Trm[47]	STT	0.0214	0	0.2426	0.0957	1.0504	0.7247	0.0231
PriorMotion(Ours)	STT	0.0267	0	0.2341(↓3.51%)	0.0949	0.9136(↓13.02%)	0.5738	0.0094
STI[44]	STI	0.0244	0	0.2375	0.0950	0.9078	0.6262	0.0221
BE-STI[44] \dagger	STI	0.0220	0	0.2115	0.0929	0.7511	0.5413	0.0108
PriorMotion(Ours)	STI	0.0273	0	0.2207(↓7.07%)	0.0931	0.7287 (↓19.73%)	0.5329	0.0075

Table 1. Comparison with State-of-the-Art Results on nuScenes. We report the mean errors for static grids, moving grids with speed $\leq 5\text{m/s}$, and moving grids with speed $> 5\text{m/s}$. Pillar.M(I&L)[25] is the only method trained using both camera and LiDAR modalities. \dagger : MGDA [30]. \ddagger : Data augmentation from [43]. STPN: MotionNet backbone. STT: ST-Trm backbone. STI: BE-STI backbone.

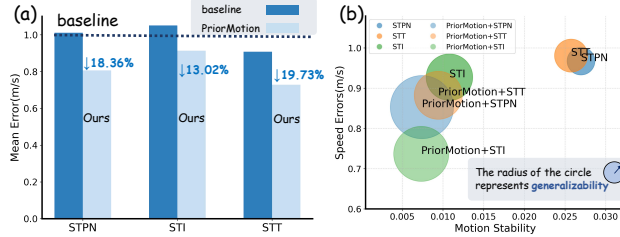


Figure 5. Our methods outperforms the baseline across both (a) traditional mean speed error($>5\text{m/s}$) and (b) newly proposed metrics. The radius of the circle represents generalization ability.

of 5 frames, with the last frame corresponding to the current time and the previous 4 frames from past timestamps. During training, we supervise the model with both motion prediction and cell classification tasks. We use the Adam optimizer [16] with an initial learning rate of 0.0016, which is decayed by a factor of 0.5 at epochs 10, 20, 30, and 40. The network is trained for 45 epochs with a batch size of 4 on a single Tesla A100 GPU.

Evaluation metrics. To evaluate our model’s performance, we follow the protocol established in [49]. This includes dividing non-empty cells into three speed groups (static: speed $\leq 0.2\text{m/s}$, slow: speed $\leq 5\text{m/s}$, and fast: speed $> 5\text{m/s}$) and reporting the mean and median prediction errors for each group. We also report overall accuracy (OA) and mean category accuracy (MCA) for cell classification tasks. Detailed metrics and calculations are provided in the supplementary material. To comprehensively assess our model, we introduce several novel metrics:

Generalization metric. We evaluate the model’s ability

to generalize to unseen categories by masking the loss for a specific category during training, preventing the model from optimizing its predictions for that category. At test time, we measure the displacement error exclusively for the masked category. Let M be the set of masked cells, and \hat{v}_i and v_i be the predicted and ground truth velocities for cell i , respectively. The error for the masked cells and generalization index (GI) is defined as:

$$L_{M_c} = \frac{1}{|M|} \sum_{i \in M} \|\hat{v}_i - v_i\|_2, \quad GI = \frac{L_{M_c}^{\text{Mask}}}{L_{M_c}} \quad (11)$$

where $L_{M_c}^{\text{Mask}}$ is the error for the masked category in the masked training scenario, and L_{M_c} is the error for the same category without masking. A higher GI indicates better generalization.

Motion stability metric. This metric measures the stability of motion predictions for grids belonging to the same instance. We calculate the variance of the displacement vectors for grids associated with the same instance. Let \mathcal{I} be the set of instances, and D_i be the set of displacement vectors for instance i . The velocity stability for instance i is:

$$\sigma_i^2 = \frac{1}{|D_i|} \sum_{d \in D_i} \|d - \bar{d}_i\|_2^2 \quad (12)$$

where \bar{d}_i is the mean displacement vector for instance i .

Distance-based displacement error metric. We evaluate the model’s performance on displacement prediction across different distance intervals. We define three intervals: $[0, 10]$, $[10, 20]$, and $[20, \infty)$ meters.

Method	Classification Accuracy(%) \dagger						
	Bg	Vehicle	Ped.	Bike	Others	MCA	OA
PointRCNN[35]	98.4	78.7	44.1	11.9	44.0	55.4	96.0
LSTM-ED[29]	93.8	91.0	73.4	17.9	71.7	69.6	92.8
MotionNet[49]	97.6	90.7	77.2	25.8	65.1	71.3	96.3
MotionNet \dagger [49]	97.0	90.7	77.7	19.7	66.3	70.3	95.8
BE-STI[44]	97.3	91.1	78.6	24.5	66.5	71.6	96.0
BE-STI \dagger [44] \dagger	94.6	92.5	82.9	25.9	77.3	74.7	93.8
ST-Trm[47]	96.7	90.5	79.0	21.1	67.6	71.0	95.5
PriorMotion(Ours)	94.5	91.6	85.5	30.4	79.2	76.2	93.6

Table 2. Performance on the auxiliary cell classification task on nuScenes. The backbone used in PriorMotion is STPN.

4.2. Main Results

Comparison with SOTA methods. We compare our proposed method with several state-of-the-art (SOTA) approaches on the motion prediction task using the nuScenes dataset. In Fig.5, our method is compatible with different backbones and demonstrates significant improvements on both traditional metrics and the newly proposed ones. For fairness, no data augmentation or multi-gradient descent algorithm (MGDA) is used.

Our PriorMotion framework achieves SOTA performance across various metrics, particularly in predicting both slow and fast-moving objects, as shown in Table 1. It is compatible with multiple backbones, including STPN, STT, and STI, consistently improving performance. Specifically, our method reduces the mean prediction error by 4.18% for slow-moving objects and 18.36% for fast-moving objects compared to the MotionNet baseline. Additionally, our approach enhances the stability of motion predictions, making it robust across different scenarios. For the cell classification task, PriorMotion demonstrates superior accuracy, particularly in classifying dynamic objects like bicycles and pedestrians, further showcasing its effectiveness in complex traffic environments.

Generalization analysis. Object-level methods perform poorly under masking, delivering random-like outcomes due to their reliance on detection, tracking, and prediction pipelines. Masking regions significantly degrades detection accuracy, which cascades into the tracking and prediction stages. As a result, these methods are highly sensitive to masked objects. In contrast, class-agnostic methods, including our framework, demonstrate stronger generalization even when the loss is not propagated through masked regions during training. This is due to our generative architecture, which captures abstract prior knowledge, allowing the model to generalize more effectively to unseen scenarios, including those with masked regions.

Prediction performance at distant region. We further evaluate PriorMotion across different distance ranges. The results show a significant reduction in prediction errors at longer distances ($>20m$) compared to other methods. Traditional approaches focus primarily on encoder design and rely solely on point cloud data, which becomes sparse at

Method	Backbone	Mean Speed \downarrow		Generalization(%) \downarrow
		$\leq 5(m/s)$	$> 5(m/s)$	
MotionNet	STPN	0.0704	0.2579	
MotionNet \dagger	STPN	0.0927	0.3159	81.6
PriorMotion	STPN	0.0674	0.1969	86.4(+5.88%)
PriorMotion \dagger	STPN	0.0669	0.2278	
ST-Trm	STT	0.0822	0.3014	
ST-Trm \dagger	STT	0.0945	0.3658	82.4
PriorMotion	STT	0.0747	0.2382	84.5(+2.54%)
PriorMotion \dagger	STT	0.0855	0.2819	
BE-STI	STI	0.0736	0.2077	
BE-STI \dagger	STI	0.0744	0.2463	84.3
PriorMotion	STI	0.0615	0.1672	
PriorMotion \dagger	STI	0.0637	0.1956	85.4(+1.30%)

Table 3. Evaluation of the proposed new metrics. We report the mean errors for different speed categories and the General Index (%). The \dagger symbol denotes that the "other" category cells are masked during training.

greater distances. In contrast, our generative model integrates prior knowledge from the motion field, compensating for the sparsity of point cloud data at long ranges.

Method	Backbone	Static		Speed $\leq 5m/s$		Speed $> 5m/s$	
		Mean \downarrow	Median \downarrow	Mean \downarrow	Median \downarrow	Mean \downarrow	Median \downarrow
MotionNet	STPN	0.0224	0	0.2587	0.0957	1.2990	0.8473
PriorMotion	STPN	0.0267	0	0.2279	0.0954	0.8529	0.6546
ST-Trm	STT	0.0210	0	0.2614	0.1030	0.9809	0.7186
PriorMotion	STT	0.0243	0	0.2491	0.0952	0.9247	0.6893
STI	STI	0.0215	0	0.2784	0.09841	1.1200	0.7239
PriorMotion	STI	0.0254	0	0.1922	0.0836	0.7368	0.6261

Table 4. Comparison of SOTA methods on long-distance speed error metrics.

Runtime analysis. For real-time autonomous driving, LiDAR point cloud processing must stay within 100ms. Our model runs at 75ms on a single RTX3090 GPU, with 12ms for point cloud voxelization and 63ms for the forward pass, making it suitable for real-time applications.

Qualitative results. Qualitative results are shown in Fig. 6. Our PriorMotion framework is able to accurately predict motion across diverse object categories, and dramatically improve the motion stability and prediction ability at distance region.

4.3. Ablation Study

We conduct extensive ablation studies to evaluate the contribution of different components in our framework.

Effect of RVpE. To validate the effectiveness of the RVpE, we experiment with a simple generative framework(Simple.G), using concatenation to fuse prior knowledge. Incorporating the Rasterized and Vectorized prior representations individually and jointly—improves performance(shown in Fig.5). Specifically, adding VpE alone reduces the mean prediction error for fast-moving objects by 1.57%, as it captures instance-level prior knowledge

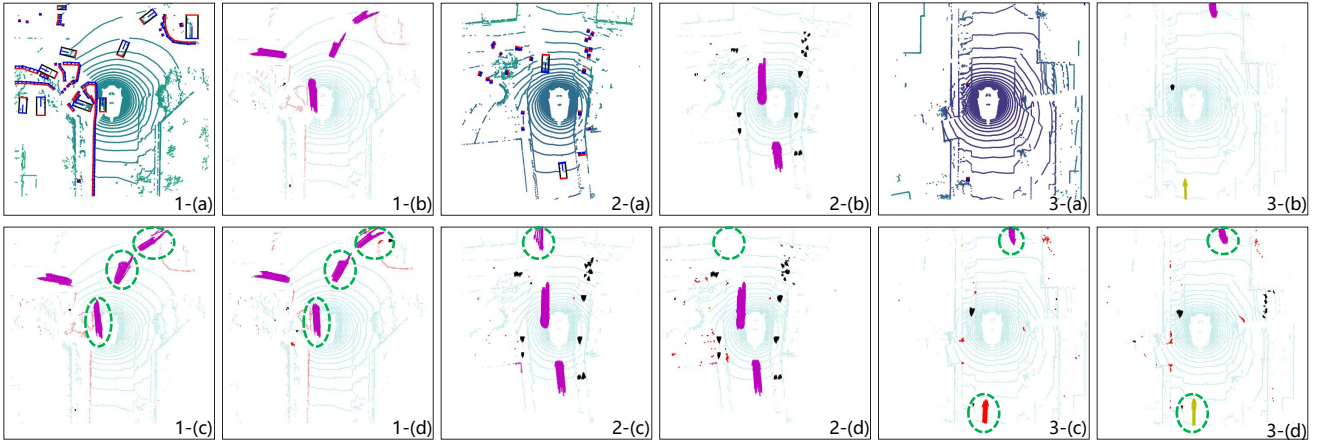


Figure 6. Comparison of qualitative results of the proposed PriorMotion and baseline model. **Top row:** (a) object-level ground truth(GT) in BEV; (b) grid-level GT **Bottom row:** (c)baseline model predictions; (d)PriorMotion predictions. We represent the motions with an arrow attached to each grid. The cell classification result is represented by various colors. Cyan: background; pink: vehicle; black: pedestrian; yellow: bike; red: others.

Method	Module			Static		Speed \leq 5m/s		Speed $>$ 5m/s	
	VpE	RpE	STpG	Mean \downarrow	Median \downarrow	Mean \downarrow	Median \downarrow	Mean \downarrow	Median \downarrow
Simple.G	X	X	X	0.0255	0	0.2477	0.0974	0.9733	0.7052
(a)	✓	X	X	0.0318	0	0.2464	0.0960	0.9580	0.7003
(b)	X	✓	X	0.2686	0	0.2356	0.0949	0.9241	0.6115
(c)	X	✓	✓	0.0274	0	0.2273	0.0953	0.8463	0.6216
(d)	✓	✓	✓	0.0285	0	0.2364	0.0893	0.8064	0.5869

Table 5. Performance comparison of our models with different combinations of components on nuScenes. Simple.G is designed with the simple generative framework. The models listed here are implemented without MGDA[30] for purely evaluation of components.

from vectorized representations, enhancing dynamic motion modeling. However, static cells show a slight performance drop due to the sparse nature of vector priors.

RpE further reduces the mean prediction error by 4.88% for slow-moving and 5.05% for fast-moving objects. By extracting prior knowledge from rasterized representations, RpE offers global, spatially consistent cues that complement VpE. The combination of both modules yields the most significant overall improvement, especially in motion stability, highlighting the benefit of integrating raster and vector priors for comprehensive scene understanding.

Effect of STpG. We also assess the role of the Spatio-Temporal Gating (STpG) mechanism, focusing on the Spatial GRU (SGRU). As shown in Table 5, removing SGRU leads to a notable performance drop, underscoring its importance in capturing spatial dependencies and maintaining temporal coherence in the motion field. While SGRU may introduce some complexity, leading to potential overfitting in static regions, it remains essential for effectively modeling the temporal dynamics of moving objects.

Performance on our private dataset. We further evaluate PriorMotion’s performance on a private dataset collected using FMCW LiDAR. Our method shows consistent improvements in motion stability and speed accuracy in distant regions, demonstrating robustness across diverse sce-

narios. Detailed results are provided in the appendix.

5. Conclusion

We have introduced **PriorMotion**, a novel framework for class-agnostic motion prediction in autonomous driving that leverages spatial and temporal priors through the **RVpE** and **STpG** modules. The RVpE module effectively extracts prior knowledge by fusing rasterized and vectorized representations, and the STpG module subsequently models spatio-temporal Gaussian distributions to capture dynamic patterns. This generative framework enables more accurate and robust predictions, achieving state-of-the-art performance on standard metrics and excelling on our newly introduced metrics for comprehensive evaluation. We believe PriorMotion will significantly advance autonomous driving technologies, particularly in open and complex environments.

References

- [1] Mayank Bansal, Alex Krizhevsky, and Abhijit Ogale. Chauffeurnet: Learning to drive by imitating the best and synthesizing the worst. *arXiv preprint arXiv:1812.03079*, 2018. 1
- [2] Jonas Becker, Jan Philip Wahle, Bela Gipp, and Terry Ruas. Text generation: A systematic literature review of tasks, eval-

uation, and challenges. *arXiv preprint arXiv:2405.15604*, 2024. 2

[3] Rishiraj Biswas, Thirumurugan Shanmugam, Rajiv Vincent, Arun Kumar Sivaraman, Janakiraman Nithiyanantham, and Priya Ravindran. Gan-enhanced multiclass malware classification with deep convolutional networks. In *Applications and Techniques in Information Security*, pages 244–255, Singapore, 2025. Springer Nature Singapore. 2

[4] Holger Caesar, Varun Bankiti, Alex H Lang, Sourabh Vora, Venice Erin Liong, Qiang Xu, Anush Krishnan, Yu Pan, Giacomo Baldan, and Oscar Beijbom. nuscenes: A multi-modal dataset for autonomous driving. In *Proceedings of the IEEE/CVF conference on computer vision and pattern recognition*, pages 11621–11631, 2020. 5

[5] Ming-Fang Chang, John Lambert, Patsorn Sangkloy, Jagjeet Singh, Slawomir Bak, Andrew Hartnett, De Wang, Peter Carr, Simon Lucey, Deva Ramanan, et al. Argoverse: 3d tracking and forecasting with rich maps. In *Proceedings of the IEEE/CVF conference on computer vision and pattern recognition*, pages 8748–8757, 2019. 1

[6] Nemanja Djuric, Vladan Radosavljevic, Henggang Cui, Thi Nguyen, Fang-Chieh Chou, Tsung-Han Lin, Nitin Singh, and Jeff Schneider. Uncertainty-aware short-term motion prediction of traffic actors for autonomous driving. In *Proceedings of the IEEE/CVF Winter Conference on Applications of Computer Vision*, pages 2095–2104, 2020. 1

[7] Scott Ettinger, Kratarth Goel, Avikalp Srivastava, and Rami Al-Rfou. Scaling motion forecasting models with ensemble distillation. *arXiv preprint arXiv:2404.03843*, 2024. 2

[8] Liangji Fang, Qinhong Jiang, Jianping Shi, and Bolei Zhou. Tpnet: Trajectory proposal network for motion prediction. In *Proceedings of the IEEE/CVF Conference on Computer Vision and Pattern Recognition*, pages 6797–6806, 2020. 1

[9] Shaoheng Fang, Zuhong Liu, Mingyu Wang, Chenxin Xu, Yiqi Zhong, and Siheng Chen. Self-supervised bird’s eye view motion prediction with cross-modality signals. In *Proceedings of the AAAI Conference on Artificial Intelligence*, pages 1726–1734, 2024. 1

[10] Tai Fei, SC Mukhopadhyay, João Paulo Javidi Da Costa, Chirasree RoyChaudhuri, Lan Lan, and Nevine Demitri. Spatial environment perception and sensing in automated systems: A review. *IEEE Sensors Journal*, 2024. 1

[11] Xiye Gu, Yijie Wang, Chongruo Wu, Yong Jae Lee, and Panqu Wang. Hplflownet: Hierarchical permutohedral lattice flownet for scene flow estimation on large-scale point clouds. In *Proceedings of the IEEE/CVF conference on computer vision and pattern recognition*, pages 3254–3263, 2019. 6

[12] Agrim Gupta, Justin Johnson, Li Fei-Fei, Silvio Savarese, and Alexandre Alahi. Social gan: Socially acceptable trajectories with generative adversarial networks. In *Proceedings of the IEEE conference on computer vision and pattern recognition*, pages 2255–2264, 2018. 2

[13] Jie Hu, Li Shen, and Gang Sun. Squeeze-and-excitation networks. In *Proceedings of the IEEE conference on computer vision and pattern recognition*, pages 7132–7141, 2018. 5

[14] Peijin Jia, Tuopu Wen, Ziang Luo, Mengmeng Yang, Kun Jiang, Ziyuan Liu, Xuewei Tang, Zhiqian Lei, Le Cui, Bo Zhang, et al. Diffmap: Enhancing map segmentation with map prior using diffusion model. *IEEE Robotics and Automation Letters*, 2024. 2

[15] Margret Keuper, Siyu Tang, Bjoern Andres, Thomas Brox, and Bernt Schiele. Motion segmentation & multiple object tracking by correlation co-clustering. *IEEE transactions on pattern analysis and machine intelligence*, 42(1):140–153, 2018. 2

[16] Diederik P. Kingma and Jimmy Ba. Adam: A method for stochastic optimization, 2017. 6

[17] Alex H Lang, Sourabh Vora, Holger Caesar, Lubing Zhou, Jiong Yang, and Oscar Beijbom. Pointpillars: Fast encoders for object detection from point clouds. In *Proceedings of the IEEE/CVF conference on computer vision and pattern recognition*, pages 12697–12705, 2019. 2

[18] Yann LeCun. A path towards autonomous machine intelligence version 0.9. 2, 2022-06-27. *Open Review*, 62(1):1–62, 2022. 1

[19] Stéphanie Lefèvre, Dizan Vasquez, and Christian Laugier. A survey on motion prediction and risk assessment for intelligent vehicles. *ROBOMECH journal*, 1:1–14, 2014. 2

[20] Jesse Levinson, Jake Askeland, Jan Becker, Jennifer Dolson, David Held, Soeren Kammel, J Zico Kolter, Dirk Langer, Oliver Pink, Vaughan Pratt, et al. Towards fully autonomous driving: Systems and algorithms. In *2011 IEEE intelligent vehicles symposium (IV)*, pages 163–168. IEEE, 2011. 1

[21] Ruibo Li, Hanyu Shi, Ziang Fu, Zhe Wang, and Guosheng Lin. Weakly supervised class-agnostic motion prediction for autonomous driving. In *Proceedings of the IEEE/CVF Conference on Computer Vision and Pattern Recognition*, pages 17599–17608, 2023. 2

[22] Jinhao Liang, Chaopeng Tan, Longhao Yan, Jingyuan Zhou, Guodong Yin, and Kaidi Yang. Interaction-aware trajectory prediction for safe motion planning in autonomous driving: A transformer-transfer learning approach. *arXiv preprint arXiv:2411.01475*, 2024. 1

[23] Ming Liang, Bin Yang, Wenyuan Zeng, Yun Chen, Rui Hu, Sergio Casas, and Raquel Urtasun. Pnpnet: End-to-end perception and prediction with tracking in the loop. In *Proceedings of the IEEE/CVF Conference on Computer Vision and Pattern Recognition*, pages 11553–11562, 2020. 1

[24] Xingyu Liu, Charles R Qi, and Leonidas J Guibas. Flownet3d: Learning scene flow in 3d point clouds. In *Proceedings of the IEEE/CVF conference on computer vision and pattern recognition*, pages 529–537, 2019. 6

[25] Chenxu Luo, Xiaodong Yang, and Alan Yuille. Self-supervised pillar motion learning for autonomous driving. In *Proceedings of the IEEE/CVF Conference on Computer Vision and Pattern Recognition*, pages 3183–3192, 2021. 2, 6

[26] Aditya Prakash, Kashyap Chitta, and Andreas Geiger. Multi-modal fusion transformer for end-to-end autonomous driving. In *Proceedings of the IEEE/CVF conference on computer vision and pattern recognition*, pages 7077–7087, 2021. 1

[27] Charles R Qi, Hao Su, Kaichun Mo, and Leonidas J Guibas. Pointnet: Deep learning on point sets for 3d classification

and segmentation. In *Proceedings of the IEEE conference on computer vision and pattern recognition*, pages 652–660, 2017. 2

[28] Charles Ruizhongtai Qi, Li Yi, Hao Su, and Leonidas J Guibas. Pointnet++: Deep hierarchical feature learning on point sets in a metric space. *Advances in neural information processing systems*, 30, 2017. 2

[29] Marcel Schreiber, Stefan Hoermann, and Klaus Dietmayer. Long-term occupancy grid prediction using recurrent neural networks. In *2019 International Conference on Robotics and Automation (ICRA)*, pages 9299–9305. IEEE, 2019. 1, 2, 6, 7

[30] Ozan Sener and Vladlen Koltun. Multi-task learning as multi-objective optimization. *Advances in neural information processing systems*, 31, 2018. 6, 8

[31] Amirreza Shaban, Xiangyun Meng, JoonHo Lee, Byron Boots, and Dieter Fox. Semantic terrain classification for off-road autonomous driving. In *Conference on Robot Learning*, pages 619–629. PMLR, 2022. 1

[32] Pourya Shamsolmoali, Masoumeh Zareapoor, Eric Granger, Huiyu Zhou, Ruili Wang, M Emre Celebi, and Jie Yang. Image synthesis with adversarial networks: A comprehensive survey and case studies. *Information Fusion*, 72:126–146, 2021. 2

[33] Sarthak Sharma, Junaid Ahmed Ansari, J Krishna Murthy, and K Madhava Krishna. Beyond pixels: Leveraging geometry and shape cues for online multi-object tracking. In *2018 IEEE International Conference on Robotics and Automation (ICRA)*, pages 3508–3515. IEEE, 2018. 2

[34] Liushuai Shi, Le Wang, Sanping Zhou, and Gang Hua. Trajectory unified transformer for pedestrian trajectory prediction. In *Proceedings of the IEEE/CVF International Conference on Computer Vision*, pages 9675–9684, 2023. 2

[35] Shaoshuai Shi, Xiaogang Wang, and Hongsheng Li. Pointrcnn: 3d object proposal generation and detection from point cloud. In *Proceedings of the IEEE/CVF conference on computer vision and pattern recognition*, pages 770–779, 2019. 7

[36] Shaoshuai Shi, Chaoxu Guo, Li Jiang, Zhe Wang, Jianping Shi, Xiaogang Wang, and Hongsheng Li. Pv-rcnn: Point-voxel feature set abstraction for 3d object detection. In *Proceedings of the IEEE/CVF conference on computer vision and pattern recognition*, pages 10529–10538, 2020. 2

[37] Yining Shi, Kun Jiang, Jiusi Li, Zelin Qian, Junze Wen, Mengmeng Yang, Ke Wang, and Diange Yang. Grid-centric traffic scenario perception for autonomous driving: A comprehensive review. *arXiv preprint arXiv:2303.01212*, 2023. 1

[38] Yining Shi, Kun Jiang, Ke Wang, Jiusi Li, Yunlong Wang, Mengmeng Yang, and Diange Yang. Streamingflow: Streaming occupancy forecasting with asynchronous multi-modal data streams via neural ordinary differential equation. In *Proceedings of the IEEE/CVF Conference on Computer Vision and Pattern Recognition*, pages 14833–14842, 2024. 2

[39] Jeany Son, Mooyeon Baek, Minsu Cho, and Bohyung Han. Multi-object tracking with quadruplet convolutional neural networks. In *Proceedings of the IEEE conference on computer vision and pattern recognition*, pages 5620–5629, 2017. 2

[40] Hao Tang, Hong Liu, Dan Xu, Philip HS Torr, and Nicu Sebe. Attentiongan: Unpaired image-to-image translation using attention-guided generative adversarial networks. *IEEE transactions on neural networks and learning systems*, 34(4):1972–1987, 2021. 2

[41] Dequan Wang, Coline Devin, Qi-Zhi Cai, Philipp Krähenbühl, and Trevor Darrell. Monocular plan view networks for autonomous driving. In *2019 IEEE/RSJ International Conference on Intelligent Robots and Systems (IROS)*, pages 2876–2883. IEEE, 2019. 1

[42] Kewei Wang, Yizheng Wu, Jun Cen, Zhiyu Pan, Xingyi Li, Zhe Wang, Zhiguo Cao, and Guosheng Lin. Self-supervised class-agnostic motion prediction with spatial and temporal consistency regularizations. In *Proceedings of the IEEE/CVF Conference on Computer Vision and Pattern Recognition*, pages 14638–14647, 2024. 2

[43] Kewei Wang, Yizheng Wu, Zhiyu Pan, Xingyi Li, Ke Xian, Zhe Wang, Zhiguo Cao, and Guosheng Lin. Semi-supervised class-agnostic motion prediction with pseudo label regeneration and bevmix. In *Proceedings of the AAAI Conference on Artificial Intelligence*, pages 5490–5498, 2024. 2, 6

[44] Yunlong Wang, Hongyu Pan, Jun Zhu, Yu-Huan Wu, Xin Zhan, Kun Jiang, and Diange Yang. Be-sti: Spatial-temporal integrated network for class-agnostic motion prediction with bidirectional enhancement. In *Proceedings of the IEEE/CVF Conference on Computer Vision and Pattern Recognition*, pages 17093–17102, 2022. 1, 2, 3, 6, 7

[45] Yuning Wang, Pu Zhang, Lei Bai, and Jianru Xue. Fend: A future enhanced distribution-aware contrastive learning framework for long-tail trajectory prediction. In *Proceedings of the IEEE/CVF Conference on Computer Vision and Pattern Recognition*, pages 1400–1409, 2023. 2

[46] Zhensong Wei, Xuewei Qi, Zhengwei Bai, Guoyuan Wu, Saswat Nayak, Peng Hao, Matthew Barth, Yongkang Liu, and Kentaro Oguchi. Spatiotemporal transformer attention network for 3d voxel level joint segmentation and motion prediction in point cloud. In *2022 IEEE Intelligent Vehicles Symposium (IV)*, pages 1381–1386. IEEE, 2022. 1

[47] Zhensong Wei, Xuewei Qi, Zhengwei Bai, Guoyuan Wu, Saswat Nayak, Peng Hao, Matthew Barth, Yongkang Liu, and Kentaro Oguchi. Spatiotemporal transformer attention network for 3d voxel level joint segmentation and motion prediction in point cloud. In *2022 IEEE Intelligent Vehicles Symposium (IV)*, pages 1381–1386. IEEE, 2022. 2, 3, 6, 7

[48] Sungmin Woo, Minjung Kim, Donghyeong Kim, Sungjun Jang, and Sangyoun Lee. Fimp: Future interaction modeling for multi-agent motion prediction. *arXiv preprint arXiv:2401.16189*, 2024. 2

[49] Pengxiang Wu, Siheng Chen, and Dimitris N Metaxas. Motionnet: Joint perception and motion prediction for autonomous driving based on bird’s eye view maps. In *Proceedings of the IEEE/CVF conference on computer vision and pattern recognition*, pages 11385–11395, 2020. 1, 2, 3, 5, 6, 7

[50] Guipeng Xin, Duanfeng Chu, Liping Lu, Zejian Deng, Yuang Lu, and Xigang Wu. Multi-agent trajectory prediction

with difficulty-guided feature enhancement network. *arXiv preprint arXiv:2407.18551*, 2024. 2

[51] Tianwei Yin, Xingyi Zhou, and Philipp Krahenbuhl. Center-based 3d object detection and tracking. In *Proceedings of the IEEE/CVF conference on computer vision and pattern recognition*, pages 11784–11793, 2021. 2

[52] Jiawei Zhang. Cognitive functions of the brain: perception, attention and memory. *arXiv preprint arXiv:1907.02863*, 2019. 1

[53] Qichao Zhang, Yinfeng Gao, Yikang Zhang, Youtian Guo, Dawei Ding, Yunpeng Wang, Peng Sun, and Dongbin Zhao. Trajgen: Generating realistic and diverse trajectories with reactive and feasible agent behaviors for autonomous driving. *IEEE Transactions on Intelligent Transportation Systems*, 23(12):24474–24487, 2022. 2

[54] Hang Zhao, Jiyang Gao, Tian Lan, Chen Sun, Ben Sapp, Balakrishnan Varadarajan, Yue Shen, Yi Shen, Yuning Chai, Cordelia Schmid, et al. Tnt: Target-driven trajectory prediction. In *Conference on Robot Learning*, pages 895–904. PMLR, 2021. 1

[55] Wenzhao Zheng, Ruiqi Song, Xianda Guo, Chenming Zhang, and Long Chen. Genad: Generative end-to-end autonomous driving. *arXiv preprint arXiv:2402.11502*, 2024. 2

[56] Qiang Zhou and Chaohui Yu. Point rcnn: An angle-free framework for rotated object detection. *Remote Sensing*, 14(11):2605, 2022. 6